

BNL-HET-04/12

FSU-HEP-2004/0804

UB-HET-04-02

hep-ph/0408077

Higgs boson production with one bottom quark jet at hadron colliders

S. Dawson

*Department of Physics, Brookhaven National Laboratory,
Upton, NY 11973-5000, USA*

C.B. Jackson, L. Reina

*Department of Physics, Florida State University,
Tallahassee, FL 32306-4350, USA*

D. Wackeroth

*Department of Physics, State University of New York at Buffalo,
Buffalo, NY 14260-1500, USA*

Abstract

We present total rates and kinematic distributions for the associated production of a single bottom quark and a Higgs boson at the Tevatron and the LHC. We include next-to-leading order QCD corrections and compare the results obtained in the four and five flavor number schemes for parton distribution functions.

Higgs boson production with one bottom quark jet at hadron colliders

S. Dawson^a, C.B. Jackson^b, L. Reina^b, and D. Wackerth^c

a) Department of Physics, Brookhaven National Laboratory, Upton, NY 11973-5000, USA

b) Physics Department, Florida State University, Tallahassee, FL 32306-4350, USA

c) Department of Physics, State University of New York, Buffalo, NY 14260-1500, USA

We present total rates and kinematic distributions for the associated production of a single bottom quark and a Higgs boson at the Tevatron and the LHC. We include next-to-leading order QCD corrections and compare the results obtained in the four and five flavor number schemes for parton distribution functions.

One of the most pressing problems of particle physics is to uncover the origin of electroweak symmetry breaking. The Standard Model (SM) predicts the existence of one scalar particle, the Higgs boson, as a consequence of the generation of gauge boson masses via the Higgs-Kibble mechanism. Extensions of the SM often introduce more Higgs fields, whose properties may drastically differ from the SM Higgs boson. Finding experimental evidence for the existence of one or more Higgs bosons and measuring their couplings to gauge bosons, leptons, and quarks is a major goal of particle physics.

In this letter, we focus on Higgs boson production in association with bottom (b) quarks. The coupling of the Higgs boson to a b quark is suppressed in the SM by the small factor m_b/v , where $v = (\sqrt{2}G_F)^{-1/2} = 246$ GeV, implying that associated production of a SM Higgs boson with b quarks is very small at both the Tevatron and the LHC. In a two Higgs doublet model or a supersymmetric model, however, this coupling is proportional to the ratio of neutral Higgs boson vacuum expectation values, $\tan\beta$, and can be significantly enhanced for large values of $\tan\beta$.

The associated production of a Higgs boson with b quarks proceeds at tree level via $q\bar{q}, gg \rightarrow b\bar{b}h$, as illustrated in Fig. 1. Fully inclusive or semi-inclusive Higgs production cross sections are then obtained by imposing no identification cuts on the final state b quarks or by requiring that at least one b quark is observed at high transverse momentum, p_T , respectively. This approach with no b quarks in the initial state is dubbed the fixed or *four flavor number scheme* (4FNS). Large logarithms of the form $\Lambda = \log(\mu_h^2/m_b^2)$ (for $\mu_h \approx M_h$) arise at all orders in α_s from the integration over the p_T of the final state b quarks that originate from the collinear splitting of an initial state gluon. In order to stabilize the perturbative expansion of the corresponding cross section, these logarithms can be resummed into a b quark perturbatively defined parton distribution function (PDF), which integrates over the low p_T region of the corresponding b quark up to scales of the order of the factorization scale. This approach is identified as the variable or *five flavor number scheme* (5FNS) [1, 2, 3]. The 5FNS is based on the approximation that the outgoing b quarks are at small p_T . It can be used only if the corresponding b quark is

treated inclusively and no p_T cut is required to identify the b quark in the final state. In the 5FNS the leading processes for fully inclusive and semi-inclusive Higgs production with b quarks are $b\bar{b} \rightarrow h$ and $bg \rightarrow bh$, respectively (the case of $bg \rightarrow bh$ is illustrated in Fig. 2, at tree level). In this approach the processes $q\bar{q}, gg \rightarrow b\bar{b}h$ are subleading contributions of higher order in the $\alpha_s^n \Lambda^m$ expansion [4, 5].

Assessing the validity and compatibility of the 4FNS and 5FNS approaches in the context of Higgs production with b quarks has recently been the subject of much theoretical interest. In this letter, we focus exclusively on the production of a Higgs boson with one identified b quark jet, and analyze in detail the results obtained within the 4FNS and 5FNS. Requiring one final state b quark measures unambiguously the Yukawa coupling of the b quark and significantly enhances the rate with respect to the case when both b quarks are identified. Higgs boson production with one b quark jet (and $h \rightarrow b\bar{b}$) has been extensively studied by the CDF and D0 collaborations [6, 7] and is going to play a major role in the experimental searches for Higgs bosons beyond the SM at the Tevatron and at the LHC. Thus, a more dedicated effort aimed at refining the theoretical predictions for both total and differential cross sections is mandatory.

A first study of the next-to-leading order (NLO) QCD total cross sections for $q\bar{q}, gg \rightarrow b\bar{b}h$ [8, 9] and for $bg \rightarrow bh$ [10] processes has been presented in Ref. [11]. In this letter we concentrate on the comparison of total and differential cross sections at NLO QCD in the 4FNS and 5FNS schemes. This is the first comparison of differential cross sections in the two PDF schemes and is important to assess the residual theoretical uncertainties in future experimental analyses. In particular, we discuss the effects of including the closed top quark loop diagram of Fig. 3, a contribution that had been previously neglected, in the NLO calculation of $bg \rightarrow bh$ in the 5FNS.

The NLO QCD corrections to $pp, p\bar{p} \rightarrow b(\bar{b})h$ production in the 4FNS consist of calculating the $\mathcal{O}(\alpha_s)$ virtual and real QCD corrections to the $q\bar{q}, gg \rightarrow b\bar{b}h$ tree level processes [8, 9], imposing identification cuts on the transverse momentum and pseudorapidity of either the b or \bar{b} final state quark (antiquark). Results from the two existing calculations [8, 9] have been compared and found



FIG. 1: Sample Feynman diagrams for $gg \rightarrow b\bar{b}h$ and $q\bar{q} \rightarrow b\bar{b}h$ production at tree level.



FIG. 2: Feynman diagrams for $gb \rightarrow bh$ production at tree level.

in good agreement (see Ref. [11]). Except for the identification cuts, the calculation is identical to that for $t\bar{t}h$ production [12, 13, 14, 15, 16, 17] with the global replacement of the top quark by the bottom quark mass ($m_t \rightarrow m_b$) and Yukawa coupling ($g_{t\bar{t}h} \rightarrow g_{b\bar{b}h}$), where m_b is always non zero.

The NLO QCD corrections to $pp, p\bar{p} \rightarrow bh + \bar{b}h$ production in the 5FNS have been presented in Ref. [10] and are encoded in the Monte Carlo program MCFM [18]. In Ref. [10], the calculation of the cross sections for $bg \rightarrow bh$ is performed in the $m_b = 0$ approximation (except for the b quark Yukawa coupling), and for this reason the only virtual diagram containing a top quark loop (see Fig. 3) is neglected. Indeed, the contribution of this diagram to the virtual cross section is proportional to $g_{t\bar{t}h}g_{b\bar{b}h}m_b/m_t$ and therefore vanishes when $m_b = 0$. At the same time, in the SM ($g_{b\bar{b}h} = m_b/v$) the contribution of this diagram is overall of order $g_{b\bar{b}h}^2$ as all other diagrams retained in the $m_b = 0$ approximation. So, it can play a relevant numerical role in the comparison between the 5FNS and the 4FNS, where diagrams with closed top quark loops are included. To investigate this issue we have computed this contribution to the $bg \rightarrow bh$ process and implemented it

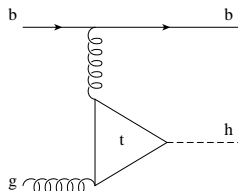


FIG. 3: Feynman diagram for the closed top quark loop contribution to $gb \rightarrow bh$.

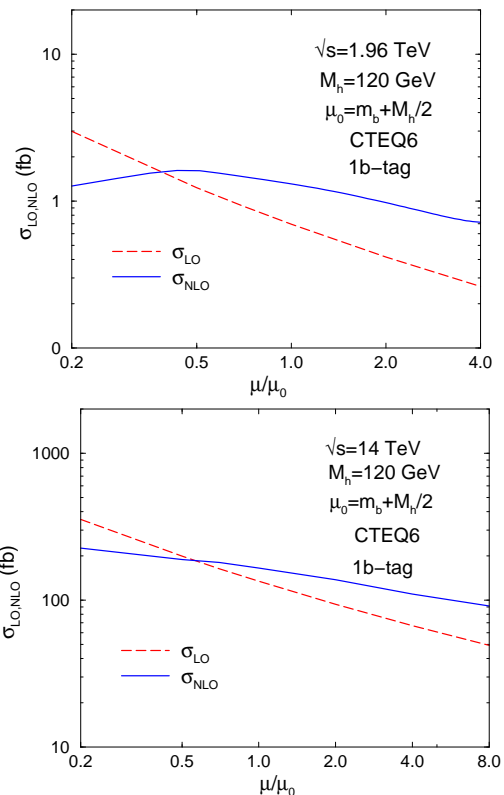


FIG. 4: Total LO and NLO cross sections for $pp, p\bar{p} \rightarrow b(\bar{b})h$ production in the 4FNS as a function of $\mu = \mu_r = \mu_f$ for $M_h = 120$ GeV, at both the Tevatron and the LHC.

into MCFM. All numerical results in the 5FNS presented here are obtained with this modified version of MCFM.

Our LO numerical results are obtained using CTEQ6L1 PDFs [19, 20] and the 1-loop evolution of α_s , while for NLO results we use CTEQ6M PDFs and the 2-loop evolution of α_s , with $\alpha_s(M_Z) = 0.118$. We use the \overline{MS} running b quark mass in the b quark Yukawa coupling, evaluated at 1- and 2-loops respectively for LO and NLO results (with pole mass $m_b = 4.62$ GeV). Our renormalization scheme decouples the top quark from the running of $m_b(\mu)$ and $\alpha_s(\mu)$ and is explained in detail in Ref. [9]. We work in the SM but the results can be straightforwardly generalized to the case of the scalar Higgs bosons of a supersymmetric extension of the SM, for instance, by replacing the SM top and bottom quark Yukawa couplings accordingly, as discussed in Ref. [9].

In order to simulate the experimental cuts, we require one of the final state b quarks to have $p_T > 20$ GeV and pseudo-rapidity $|\eta| < 2.0$ for the Tevatron and $|\eta| < 2.5$ for the LHC. In the NLO real gluon emission, the final state gluon and b quarks are considered as separate particles only if $\Delta R > 0.4$ ($\Delta R = \sqrt{(\Delta\eta)^2 + (\Delta\phi)^2}$).

In Fig. 4 we show, for $M_h = 120$ GeV, the dependence of the LO and NLO total cross sections, calculated in the 4FNS, on the arbitrary renormalization/factorization

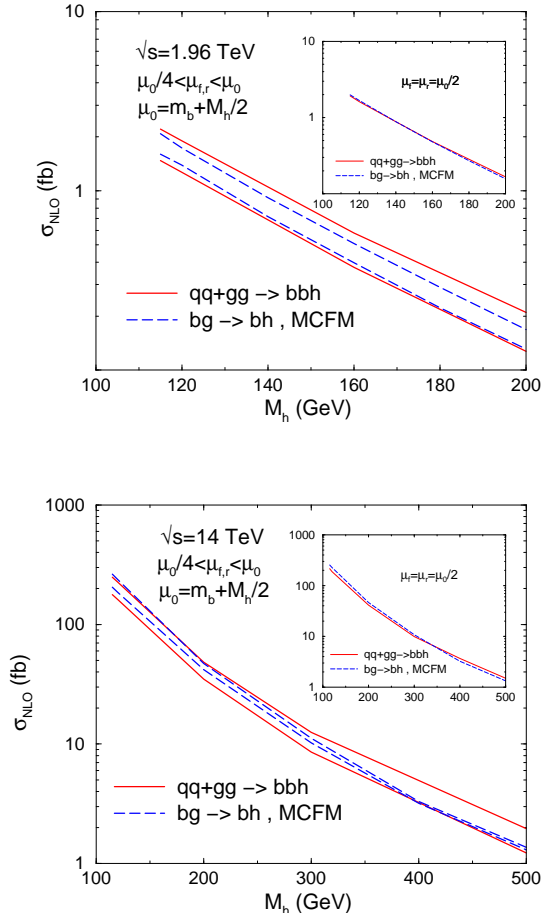


FIG. 5: Total NLO cross section for $pp, p\bar{p} \rightarrow b(\bar{b})h$ production at the Tevatron and the LHC as a function of M_h . We have assumed $\mu_r = \mu_f = \mu_0/2$ for the central curves (see inlays) and varied μ_r and μ_f independently to obtain the uncertainty bands, as explained in the text. The solid curves correspond to the 4FNS, the dashed curves to the 5FNS.

scale μ (with $\mu_r = \mu_f = \mu$). The NLO result has considerably less sensitivity to the scale choice, and the region around $\mu \approx \mu_0/2$ ($\mu_0 = m_b + M_h/2$) shows the least sensitivity to the variation of μ . For this reason we use $\mu_0/2$ as our reference scale in the following plots, whenever $\mu_r = \mu_f$. Analogous results for the 5FNS total cross sections have been presented in Ref. [10].

Fig. 5 shows the dependence of the NLO total cross sections on M_h , in both the 4FNS and 5FNS. The bands illustrate the theoretical uncertainty due to the independent variation of μ_r and μ_f about the central value $\mu_r = \mu_f = \mu_0/2$ (see inlays), between $(0.2, 0.25)\mu_0$ (4FNS, 5FNS) and μ_0 . It is extremely interesting to note that the 5FNS band is completely within the 4FNS band, and the corresponding central values are almost identical at the Tevatron and very close at the LHC. Including the closed top quark loop diagrams lowers the 5FNS cross

section (by $\approx 15\%$ at the Tevatron and $\approx 10\%$ at the LHC, when $M_h = 120$ GeV and $\mu_r = \mu_f = 0.5\mu_0$) and makes the theoretical prediction in the 4FNS and 5FNS fully compatible (see for comparison Fig. 6 in Ref. [11]). Note that the bands only give an indication of the theoretical uncertainty of each approach due to the residual scale dependence. Other sources of theoretical uncertainties, like PDF uncertainties, have not been considered.

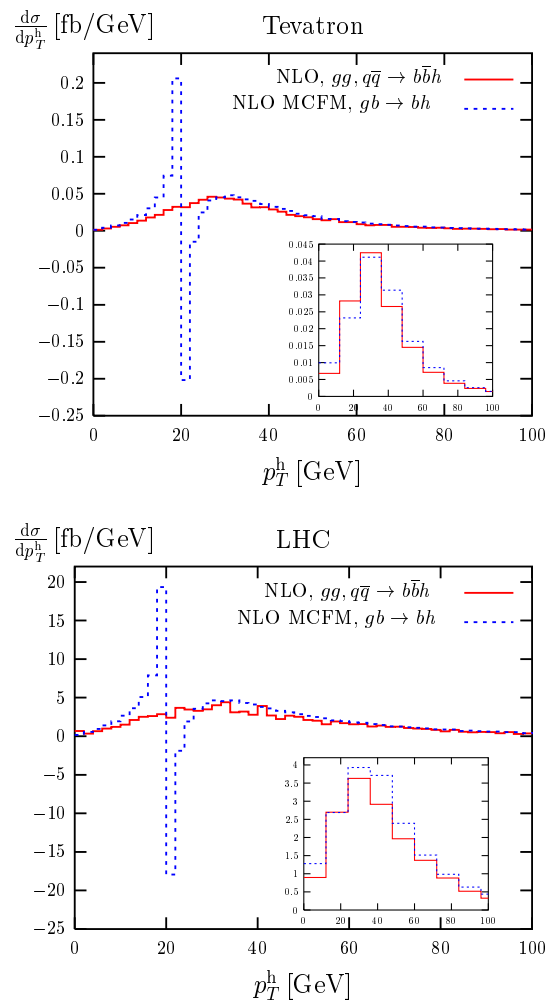


FIG. 6: $d\sigma/dp_T^h$ at the Tevatron and the LHC for $M_h = 120$ GeV and $\mu_r = \mu_f = \mu_0/2$. We show the NLO results in the 4FNS (solid) and 5FNS (dashed), using two different bin sizes, 2 GeV and 12 GeV (see inlay).

Finally, in Figs. 6-8 we compare the results for the p_T and η distributions of the Higgs boson in both the 4FNS and 5FNS, at the Tevatron and the LHC. We see, in general, a good agreement between the two schemes, except in regions of kinematical boundaries. This is particularly dramatic in the p_T^h distributions where, around $p_T^h \simeq 20$ GeV, a kinematical threshold causes the 5FNS NLO calculation to be highly unstable. This instability can be reabsorbed by using a larger bin size (see inlays),

and could therefore be interpreted as a sort of theoretical *resolution* for the 5FNS. The instabilities could be removed by a systematic resummation of threshold corrections [21, 22], but this is not implemented in MCFM. Fig. 8 illustrates the impact of NLO QCD corrections on p_T^h and η_h distributions in terms of a differential K-factor ($d\sigma_{NLO}/d\sigma_{LO}$). It is interesting to note that the 4FNS and 5FNS agree at large p_T^h but they differ substantially at low p_T^h . As can be seen in Fig. 8, there are regions of p_T^h and η_h where the NLO QCD corrections can considerably affect the shape of the distributions.

In this letter we have shown how the theoretical predictions for both total and differential cross sections for $pp, p\bar{p} \rightarrow b(\bar{b})h$ production within a 4FNS and 5FNS are fully compatible within the existing theoretical errors due to the residual normalization and factorization scale dependence at NLO in QCD. This is crucial to experimental searches based on $b\bar{b}h$ production when only one b quark jet is identified.

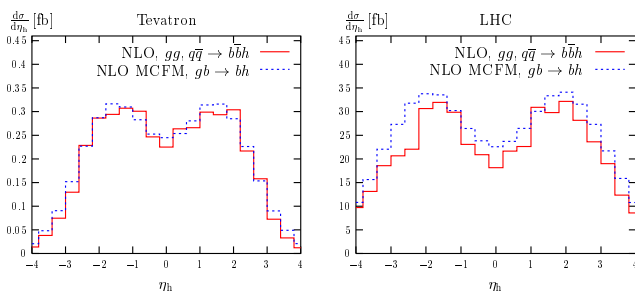


FIG. 7: $d\sigma/d\eta_h$ at the Tevatron and the LHC for $M_h = 120$ GeV and $\mu_r = \mu_f = \mu_0/2$. We show the NLO results in the 4FNS (solid) and 5FNS (dashed).

Acknowledgments

We thank S. Dittmaier, M. Krämer, and M. Spira for comparing results and J. Campbell, F. Maltoni, and S. Willenbrock for discussions. We are particularly grateful to J. Campbell for his help with the MCFM program. The work of S.D. (L.R., C.B.J.) and D.W. is supported in part by the U.S. Department of Energy under grant DE-AC02-76CH00016 (DE-FG02-97ER41022) and by the National Science Foundation under grant NSF-PHY-0244875, respectively.

[1] R. M. Barnett, H. E. Haber, and D. E. Soper, Nucl. Phys. **B306**, 697 (1988).
[2] F. I. Olness and W.-K. Tung, Nucl. Phys. **B308**, 813 (1988).
[3] D. A. Dicus and S. Willenbrock, Phys. Rev. **D39**, 751 (1989).
[4] D. Dicus, T. Stelzer, Z. Sullivan, and S. Willenbrock, Phys. Rev. **D59**, 094016 (1999), hep-ph/9811492.

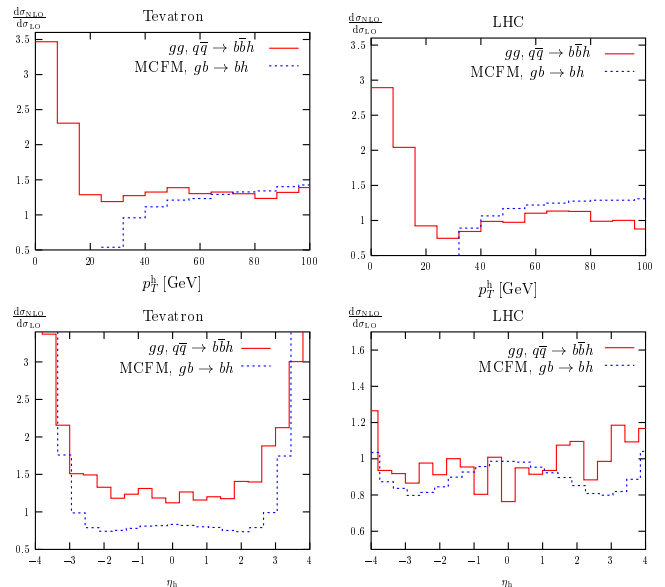


FIG. 8: The ratios of the NLO and LO p_T^h and η_h distributions at the Tevatron and the LHC for $M_h = 120$ GeV and $\mu_r = \mu_f = \mu_0/2$. We show the ratios in the 4FNS (solid) and 5FNS (dashed).

[5] C. Balazs, H.-J. He, and C. P. Yuan, Phys. Rev. **D60**, 114001 (1999), hep-ph/9812263.
[6] T. Affolder et al. (CDF), Phys. Rev. Lett. **86**, 4472 (2001), hep-ex/0010052.
[7] D0 collaboration, Results presented at Moriond 2004.
[8] S. Dittmaier, M. Krämer, and M. Spira (2003), hep-ph/0309204.
[9] S. Dawson, C. B. Jackson, L. Reina, and D. Wackerroth, Phys. Rev. **D69**, 074027 (2004), hep-ph/0311067.
[10] J. Campbell, R. K. Ellis, F. Maltoni, and S. Willenbrock, Phys. Rev. **D67**, 095002 (2003), hep-ph/0204093.
[11] J. Campbell et al. (2004), hep-ph/0405302.
[12] W. Beenakker, S. Dittmaier, M. Krämer, B. Plümper, M. Spira, and P. Zerwas, Phys. Rev. Lett. **87**, 201805 (2001), hep-ph/0107081.
[13] W. Beenakker, S. Dittmaier, M. Krämer, B. Plümper, M. Spira, and P. Zerwas, Nucl. Phys. **B653**, 151 (2003), hep-ph/0211352.
[14] L. Reina and S. Dawson, Phys. Rev. Lett. **87**, 201804 (2001), hep-ph/0107101.
[15] L. Reina, S. Dawson, and D. Wackerroth, Phys. Rev. **D65**, 053017 (2002), hep-ph/0109066.
[16] S. Dawson, L. H. Orr, L. Reina, and D. Wackerroth, Phys. Rev. **D67**, 071503 (2003), hep-ph/0211438.
[17] S. Dawson, C. Jackson, L. H. Orr, L. Reina, and D. Wackerroth, Phys. Rev. **D68**, 034022 (2003), hep-ph/0305087.
[18] J. Campbell and R.K. Ellis, webpage: mcfm.fnal.gov.
[19] J. Pumplin et al., JHEP **07**, 012 (2002), hep-ph/0201195.
[20] D. Stump et al., JHEP **10**, 046 (2003), hep-ph/0303013.
[21] V. Del Duca, F. Maltoni, Z. Nagy, and Z. Trocsanyi, JHEP **04**, 059 (2003), hep-ph/0303012.
[22] S. Catani and B. R. Webber, JHEP **10**, 005 (1997), hep-ph/9710333.